Applied Physics Letters

High thermal conductivity of free-standing skeleton in graphene foam

Cite as: Appl. Phys. Lett. **117**, 251901 (2020); https://doi.org/10.1063/5.0032408
Submitted: 08 October 2020 . Accepted: 05 December 2020 . Published Online: 22 December 2020

Jianshu Gao, Danmei Xie, Xinwei Wang, Xin Zhang, and Yanan Yue

Applied Physics Letters ARTICLE scitation.org/journal/apl

High thermal conductivity of free-standing skeleton in graphene foam

Cite as: Appl. Phys. Lett. **117**, 251901 (2020); doi: 10.1063/5.0032408
Submitted: 8 October 2020 · Accepted: 5 December 2020 ·
Published Online: 23 December 2020

Jianshu Gao,[1] Danmei Xie,[1,a)] Xinwei Wang,[2,a)] Xin Zhang,[3] and Yanan Yue[1,4,a)]

AFFILIATIONS

[1]School of Power and Mechanical Engineering, Wuhan University, Wuhan, Hubei 430072, China
[2]Department of Mechanical Engineering, Iowa State University, Ames, Iowa 50010, USA
[3]Department of Mechanical Engineering, Boston University, Boston, Massachusetts 02215, USA
[4]Department of Mechanical and Manufacturing Engineering, Miami University, Oxford, Ohio 45056, USA

[a)]**Authors to whom correspondence should be addressed:** dmxie@whu.edu.cn; xwang3@iastate.edu; and yyue@whu.edu.cn

ABSTRACT

Due to the high-porosity structure, the low thermal transport property of graphene foam (GF) is expected. However, the interconnected skeleton can still act as excellent thermal conductor branches if phonon scattering is not severely affected in the structure of graphene flakes. Such a property has not been validated experimentally due to the difficulty in sample manipulation and the fragility of the structure. In this work, we report the characterization results of thermal properties of the free-standing skeleton in GF. Three individual skeleton samples from one GF piece are prepared under the same condition. The thermal diffusivity of GF skeletons is characterized in the range of $3.26–3.48 \times 10^{-4}$ m^2/s, and the thermal conductivity is determined to be 520–555 W/(m K), which is two orders of magnitude larger than the value of bulk GF. These high thermal conductivity values originate from the intrinsic thermal property of graphene, while the contact interfaces, wrinkled structures, and defects induced in the synthesis process do not affect the phonon transport property significantly, which proves that the three-dimensional hierarchical graphene structure can still be implemented in energy-intensive applications.

Graphene foam (GF) is a three-dimensional (3D) bulk architecture interconnected by a graphene flake network.[1,2] The superior thermal properties and surface-to-volume ratio enable the integration of GF into various nanocomposite materials to improve the thermal conductivity of the base matrix, including thermal interface materials[3] and phase change materials.[4] For example, it is found that the thermal conductivity of a GF-polymer composite is threefold of the pure polymer, which is also 20% higher than that of the graphene–polymer composite with the same load.[5] However, the porous structure of GF is assembled by the interconnection of graphene flakes with random skeleton alignment. The evaluation of intrinsic thermal transport behavior in GF is beneficial for application in industrial equipment.

A flexible 3D thermal circuit network is established in describing the thermal transport in porous GF, indicating several orders of magnitude reduction in effective thermal properties compared to those of suspended monolayer graphene.[6] Pettes *et al.*[7] applied a steady-state electrical heating method to characterize the thermal properties of GF. The thermal conductivity of porous GF is calculated to be 0.26–1.7 W/(m K). The thermal conductivity experiences a decreasing trend upon elevating the temperature above 200 K, which reveals that the phonon–phonon scattering mode dominates the phonon scattering process. However, the free-standing GF skeleton could serve as an efficient heat dissipation network despite the diminution of effective thermal transport behavior in bulk GF.[8] The model from the study by Schuetz and Glicksman[9] presents a correlation between the thermal conductivity of the skeleton and bulk material by assuming a uniform assembly in geometry and the structure, which is demonstrated as valid in open-cell metal foams with porosity in the range of 0.88–0.98.[10] Li *et al.*[11] extended the model for calculating the thermal conductivity of the skeleton from the measurement results of bulk GF. The thermal conductivity of the skeleton in estimation is one order of magnitude lower than that of monolayer graphene due to the intense phonon scattering at the contact interfaces and defect points. Xie *et al.*[12] decoupled the defect level in bulk GF to obtain the ideal thermal conductivity and thermal diffusivity of the skeleton from the model in the temperature range of 33–299 K. The estimated thermal conductivity of the skeleton decreases from $\sim 10^5$ W/(m K) to 300 W/(m K) upon increasing the temperature from 80 K to room temperature. However, due to the fragility of the GF structure, there is no direct experimental characterization of the thermal properties of

the individual skeleton yet.[13] The heat transfer of graphene flakes in GF is anisotropic, which is different from the homogeneous hypothesis in metal foam. Large uncertainty could be induced into the theoretical prediction about the thermal properties of the skeleton from bulk GF.

In this work, we report the experimental study of the intrinsic thermal properties of the free-standing GF skeleton. Three individual skeleton samples are separated from the same GF piece for thermal characterization. Thermal diffusivity and thermal conductivity of the skeleton are determined at room temperature, which demonstrate the effective heat dissipation network of the skeleton in porous GF. The results are compared with those monolayer graphene to uncover the mechanism of thermal transport in the GF skeleton.

The GF sample is purchased from the Nanjing JCNANO Technology Corporation, which is synthesized by a conventional chemical vapor deposition method.[14,15] Figure 1(a) presents the scanning electron microscopy (SEM) image of the bulk GF. The three-dimensional interconnection architects a complex porous structure. The pore size of the GF is determined to be around 200 μm as shown in Fig. 1(b). In Fig. 1(c), it is found that the GF skeleton consists of large amounts of graphene flakes. The wrinkled structures and contact interfaces construct a fluctuating surface upon the GF skeleton as illustrated in Fig. 1(d). Raman characterization is implemented on the GF skeleton with an excitation laser of 532 nm. As shown in Fig. 1(e), the intensity of the D peak (1352 cm^{-1}) is around 6.8% of that of the G peak (1581 cm^{-1}). I_D/I_G determines an average crystallite size of 283 nm in the GF skeleton by using the formula $L_a(\mathrm{nm}) = (2.4 \times 10^{-10})\lambda(\mathrm{nm})^4 (I_D/I_G)^{-1}$, where L_a is the average crystallite size and λ is the excitation laser wavelength in the Raman measurement.[16] The 2D peak consists of only one Lorentzian component, indicating a typical out-of-plane staking mode of the graphene layer as that in turbostratic graphite.[17] I_{2D}/I_G is close to the value of five-layer graphene.[18] Our GF sample is assembled by elements of carbon (81.54%), oxygen (12.95%), Nitrogen (0.66%), silicon (3.09%), and phosphorus (1.76%), as demonstrated in the X-ray photoelectron spectroscopy (XPS) spectrum in Fig. 1(f). A peak at 284 eV shows the presence of C=C bonding in the GF specimen.

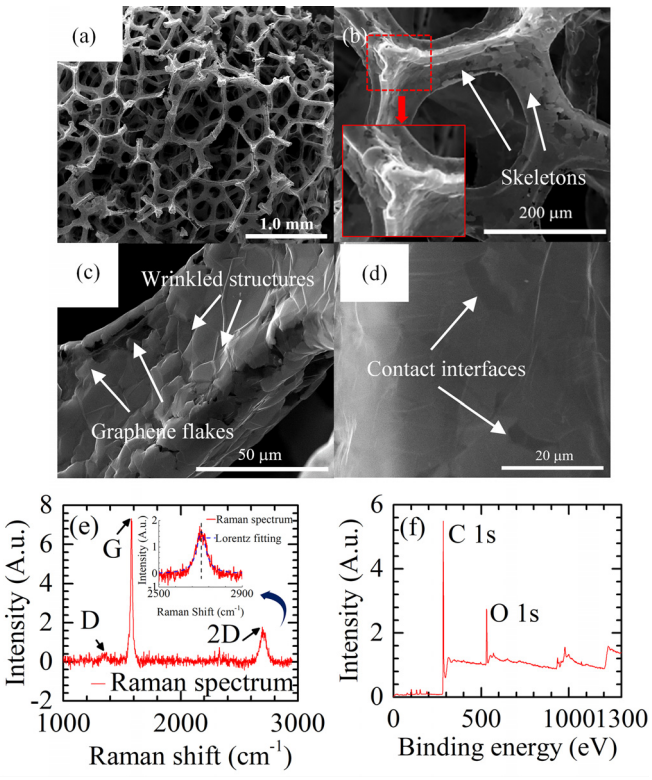

FIG. 1. SEM image of the (a) bulk GF, (b) network structure of a pore, (c) morphology upon single skeleton, (d) microscopic constituents. (e) Raman spectrum of the GF skeleton. (f) XPS spectrum of GF.

The transient electro-thermal technique (TET) is an effective method for characterizing the thermal properties of various materials.[19] Figure 2(a) illustrates the schematic setup of the thermal measurement of the GF skeleton. The sample is suspended between two aluminum electrodes in a vacuum chamber under 1 mTorr. The mean free path of the gas molecule is determined to exceed 0.05 m, which is much larger than the characteristic length of the GF skeleton to eliminate the effect of air conduction. A DC step current (from 18.0 to 29.5 mA) is applied by a current source (KEITHLEY 6220) to introduce Joule heating, which is generated inside the sample and dissipates to electrodes through heat conduction. During the heating process, the temperature rise along the sample is below 5 K so that the radiative heat loss is in a small proportion. The one-dimensional heat conduction equation with a uniform heat source is obtained as $\partial(\rho c_p T)/\partial t = k\partial^2 T/\partial x^2 + q_0$, where ρ, c_p, and k are the density, specific heat capacity, and thermal conductivity, respectively, and q_0 represents the electrical heating power per unit volume. The average temperature of sample is determined by solving the partial differential equation and is obtained as[20]

$$T(t) = T_0 + \frac{8q_0L^2}{k\pi^4}\sum_{m=1}^{\infty}\frac{1-\exp\left[-(2m-1)^2\pi^2\alpha t/L^2\right]}{(2m-1)^4}, \quad (1)$$

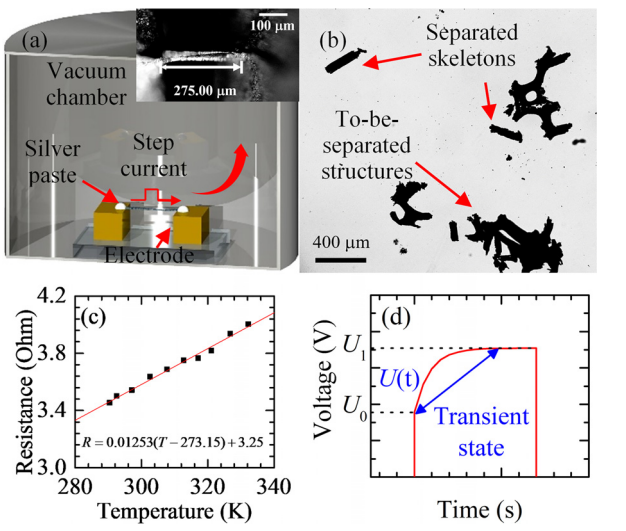

FIG. 2. (a) Schematic setup of thermal characterization of the GF skeleton. (b) Separation of the skeleton in an optical microscope view. (c) Linear fitting of the resistance of the GF skeleton with respect to temperature. (d) Transient state of voltage evolution to determine the thermal diffusivity.

where $T(t)$ is the temperature at time t, T_0 is the room temperature, L is the sample length, and α is the thermal diffusivity. The normalized temperature rise is defined in the form of $T^* = [T(t) - T_0]/[T(t \to \infty) - T_0]$ and is given as

$$T^* = \frac{96}{\pi^4} \sum_{m=1}^{\infty} \frac{1 - \exp\left[-(2m-1)^2 \pi^2 \alpha t / L^2\right]}{(2m-1)^4}. \quad (2)$$

Since the sample resistance is sensitive to temperature, the normalized temperature rise can be calculated from voltage variation, which is described as $[U(t) - U_0]/(U_1 - U_0)$, where $U(t)$, U_0, and U_1 are the voltage at time t, initial, and steady-state voltages, respectively. The thermal diffusivity can be calculated using Eq. (2) as the normalized temperature rise is obtained. The fluctuating morphology of the surface on the GF skeleton indicates that the local cross-sectional area is inconsistent along the length direction of the GF skeleton. Even if there does exist a difference in the local cross-sectional area, the surface roughness is much smaller than the skeleton width. The thermal properties in thermal characterization represent the overall thermal behavior in the GF skeleton.

In order to characterize the thermal properties of a single free-standing GF skeleton, it is necessary to separate it from the bulk foam structure. Figure 2(b) displays an optical microscope view of the separated GF skeletons and the to-be-separated structures. Due to the fragile structure of the GF skeleton, it is easy to damage the sample during the separation process from the bulk foam materials. Under careful implementation, the individual GF skeleton is separated with tungsten needles and further used in thermal characterization. The skeleton ends are glued to the electrodes with silver paste to minimize the electrical and thermal contact resistance. The experimental equipment was also verified and calibrated by measuring the thermal diffusivity and thermal conductivity of a platinum wire. The overall resistance of the platinum wire is 3.7 Ω, and the contact resistance introduced from silver paste is 0.3 Ω. The difference between the measured results and standard parameters is less than 5%. The amount of silver paste is precisely controlled by a stepper motor integrated with an injector. During this process, the surface tension from silver paste could lift up the GF skeleton and break the suspended bridge structure. To eliminate the surface tension effect from silver paste, anhydrous alcohol is sprayed onto the sample in an atomized manner. The surface tension from anhydrous alcohol facilitates the attachment between the skeleton ends. Under the combined effects of surface tension from anhydrous alcohol and silver paste, the silver paste can be smeared on the skeleton ends without lifting up the skeleton. After the natural evaporation of anhydrous alcohol, a bridge structure of the GF skeleton between the electrodes is established. In the same bulk GF piece, the skeletons share a similar interconnected structure and length. Three individual GF skeletons separated from the same piece have lengths of 244 μm, 275 μm, and 339 μm, respectively. The voltage variation is recorded at a time interval of 10 μs with a data acquisition card (NI USB-6003). The temperature effect on resistance of the GF skeleton is calibrated as shown in Fig. 2(c). The electrical resistance of the skeleton increases in the controlled temperature range of 290–332 K. The calibrated temperature dependence of the resistance of the GF skeleton reveals a temperature coefficient of electrical resistance of $3.86^{+0.14}_{-0.14} \times 10^{-3}$/K. The calculated coefficient (R-square) is 0.9890, which demonstrates a good linear correlation between electrical resistance and temperature. The skeleton itself could act as a remarkable sensor for measuring the thermal properties. In Fig. 1(d), a typical voltage evolution is recorded during the heating process and beneficial for establishing the normalized temperature rise. Thermal diffusivity of the GF skeleton is then available from the normalized temperature rise based on Eq. (2).

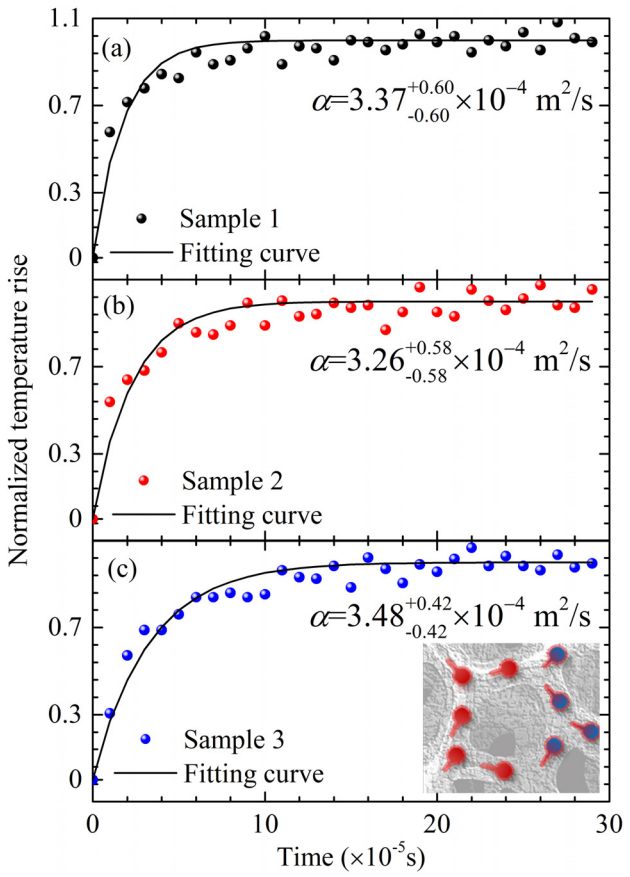

FIG. 3. Determination of thermal diffusivity from the normalized temperature rise of the GF skeleton under Joule current heating for (a) sample 1, (b) sample 2, and (c) sample 3.

Figures 3(a)–3(c) show the normalized temperature rise with respect to time for different samples. The experimental data present a similar trend in which the normalized temperature rise experiences an initial increase to a steady state. The thermal equilibrium time in the measurement takes about 1×10^{-4} s, which is extended to a longer time for a longer sample. The fitting curve is employed to determine the thermal diffusivity of the GF skeleton by using the least squares method. It is found that the thermal diffusivity varies slightly from 3.26×10^{-4} to 3.48×10^{-4} m^2/s for different samples. The uncertainty of data is from the fitting method with a confident interval of 95%. Lin *et al.*[21] carried out an experimental study to calculate the thermal properties of GF. They estimated a theoretical thermal diffusivity of the GF skeleton to be $1.16–2.22 \times 10^{-4}$ m^2/s from the measured values of bulk GF, which is in the same order of magnitude as our results.

In the TET technique, thermal conductivity can be obtained if the temperature rise and the cross-sectional area of the sample are

calculated. However, the cross section of the GF skeleton is irregular as shown in the inset of Fig. 1(b), which hinders the accurate calculation of thermal conductivity and causes large uncertainty. Due to the porosity in the bulk foam structure, there is a decrease in density in bulk GF compared to the skeleton. The intrinsic density and specific heat capacity of the GF skeleton are only sensitive to the composition materials of graphene flakes in the skeleton, but not to the porosity in bulk foam. Besides, the SEM images in Figs. 1(b) and 1(c) demonstrate the interconnected graphene network in an individual GF skeleton. Based on the thermal diffusivity and the specific heat capacity of graphene, the thermal conductivity of the GF skeleton can be determined from $k = \alpha\rho c_p$. At room temperature, the values of ρ and c_p for graphene and graphite are identical,[22] which are confirmed to be 2250 kg/m^3 and 709 J/(kg K), respectively.[23,24] Figure 4 presents the thermal diffusivity and thermal conductivity for different samples of the GF skeleton. It is found that the thermal conductivity of the skeleton is in the range of 520–550 W/(m K), which demonstrates our speculation that the skeleton establishes an effective heat dissipation network despite the low thermal conductivity in bulk GF. Yang *et al.*[25] analyzed the effective thermal conductivity of open-cell foams with different geometrical structures. Effective thermal conductivity of the foam structure is decreased as the porosity and ratio between the node and the skeleton diameter are increased. Qiu *et al.*[26] indicated that the effective thermal conductivity of the foam structure is not only sensitive to porosity but also sensitive to the inhomogeneity in the pore size. Compared to the homogeneous foam structure, the effective thermal conductivity in the foam with an inhomogeneous pore size distribution is decreased by 13.5%. Wei *et al.*[27] employed machine learning to calculate the effective thermal conductivity of the foam structure. Different from that in periodic nanoporous graphene, an unexpected enhancement of effective thermal conductivity is observed in disordered nanoporous graphene, which is attributed to the effect of the shape factor and channel factor.

Our results are smaller than the suspended monolayer graphene synthesized by the CVD method [1689–1813 W/(m K)][28] and mechanical exfoliation [~3000 W/(m K)],[29] but are closed to the five-layer graphene [~580 W/(m K)][30] and regular bulk graphite materials [~520 W/(m K)].[31] Thermal transport in the GF skeleton is attributed

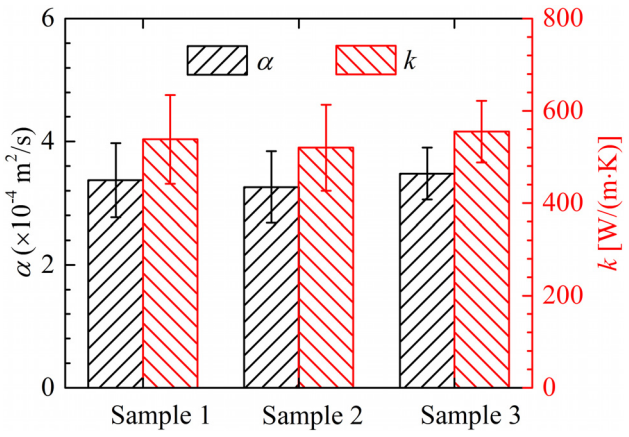

FIG. 4. Thermal diffusivity and thermal conductivity for different samples of the GF skeleton in the measurement.

to the combined effects of electron and phonon migration. The total thermal conductivity of the GF skeleton can be split into the contribution of electron migration and phonon propagation. According to the Wiedemann–Franz law, the contribution of electron migration to thermal conductivity can be calculated from $L = k_e/\sigma T$, where L is the Lorenz number, k_e is the thermal conductivity of the electron contribution, σ is the electrical conductivity, and T is the temperature. The σ value is demonstrated to be sensitive to the number of graphene layers, which could vary from 3×10^6 S/m (Ref. 32) for single-layer graphene to 1.69×10^6 S/m for graphite.[33] The maximum value of k_e can be estimated to be 22 W/(m K) with a σ value of 3×10^6 S/m at 300 K. Therefore, the electronic contribution to thermal conductivity is determined to be less than ~4% in the GF skeleton, revealing that the phonon propagation dominates the thermal transport in the GF skeleton.

As shown in the SEM image [in Fig. 1(d)], large amounts of contact interfaces between graphene flakes exist in the GF skeleton. The phonon leakage at the mismatch contact interface shortens the phonon mean free path and, thus, impedes the thermal transport in the skeleton.[34] It has been demonstrated that the thermal conductivity of polycrystalline graphene could evolve a decrease by 90% as the grain size decreases from 1000 nm to 2 nm.[35] Thermal transport is more sensitive to the phonon vibration at the contact interface in polycrystalline graphene with smaller grain sizes. Fan *et al.*[36] presented a correlation of normalized thermal conductivity at 300 K under different grain sizes with quantum correction. The normalized thermal conductivity of polycrystalline graphene (thermal conductivity ratio of polycrystalline graphene to pristine graphene) increases as the grain size is increased. When considering the average crystallite size of 283 nm in the GF skeleton as calculated from the Raman spectrum in Fig. 1(e), the normalized thermal conductivity at 300 K is determined to be 0.28 by using Fan's correlation. For a reference case of $k = 538$ W/(m K) of the GF skeleton, the thermal conductivity of pristine graphene is estimated to be 1921 W/(m K), which is comparable to the reported value.[28] Furthermore, the wrinkled structures on the surface of the GF skeleton could lead to strong phonon scattering. In our previous study of thermal transport in graphene paper,[37] a reduction of 30% in surface roughness modifies the overall thermal conductivity of graphene paper. The phonon scattering in the wrinkled structure presents a significant role in thermal transport. Besides, Fig. 2(c) shows that the electrical resistance of the GF skeleton experiences an increasing trend vs temperature within the measurement temperature range, which is different from that of monolayer graphene and few-layer graphene.[38] In all the temperature range, the electrical resistance of graphene is found to present a semiconductor-like behavior and a decrease with temperature.[39] However, when the impurity and doping phenomenon occurs in the GF skeleton, the electrical resistance could present an increasing trend as the temperature is increased.[40] The XPS spectrum of the GF skeleton in Fig. 1(f) demonstrates the defect structures induced by doped elements. The phonon density of state in doped graphene is different from that of pristine graphene.[41] Thermal conductivity of doped graphene could be decreased to 10% of pristine graphene at 300 K with a defect ratio of 0.5%. The defects in graphene reduce the relaxation time of the phonon group, leading to a suppression of thermal conductivity.

In summary, we implement an experimental study of thermal properties of the free-standing GF skeleton. The individual skeleton is separated from bulk GF for thermal characterization. Thermal

diffusivity of the skeleton is calculated to be $3.26–3.48 \times 10^{-4}$ m^2/s, and the thermal conductivity is determined in the range of 520–555 W/(m K). Different from the low thermal conductivity in bulk GF, the skeleton is demonstrated to establish an effective heat dissipation network. The results reveal that the GF skeleton experiences a moderate reduction in thermal transport compared to the monolayer graphene, which is ascribed to the presence of contact interfaces, wrinkled structures, and defects induced in the synthesis process. The three-dimensional hierarchical graphene structure is promising for the integration in energy-intensive applications.

The support from the National Natural Science Foundations of China (Nos. 52076156, 51776142, and 51727901), the Fundamental Research Funds for the Central Universities (No. 2042020kf0194), the U.S. National Science Foundation (CBET1930866), and the China Scholarship Council (No. 201906270144) is gratefully appreciated.

DATA AVAILABILITY

The data that support the findings of this study are available from the corresponding author upon request.

REFERENCES

[1]Z. Chen, W. Ren, L. Gao, B. Liu, S. Pei, and H. Cheng, Nat. Mater. **10**, 424–428 (2011).
[2]R. U. Rehman Sagar, K. Shehzad, A. Ali, F. J. Stadler, Q. Khan, J. Zhao, X. Wang, and M. Zhang, Carbon **143**, 179–188 (2019).
[3]C. Zhang, A. Li, Y. Zhao, S. Bai, and Y. Zhang, Compos. Part B **135**, 201–206 (2018).
[4]G. Qi, J. Yang, R. Bao, D. Xia, M. Cao, W. Yang, M. Yang, and D. Wei, Nano Res. **10**, 802–813 (2017).
[5]Y. Zhao, Z. Wu, and S. Bai, Compos. Part A **72**, 200–206 (2015).
[6]Q. Y. Li, K. Xia, J. Zhang, Y. Zhang, Q. Li, K. Takahashi, and X. Zhang, Nanoscale **9**, 10784–10793 (2017).
[7]M. T. Pettes, H. Ji, R. S. Ruoff, and L. Shi, Nano Lett. **12**, 2959–2964 (2012).
[8]Y. Yao, H. Wu, and Z. Liu, Int. J. Therm. Sci. **97**, 56–67 (2015).
[9]M. A. Schuetz and L. R. Glicksman, J. Cell. Plast. **20**, 114–121 (1984).
[10]S. Krishnan, J. Murthy, and S. Garimella, ASME J. Heat Transfer **128**, 793–799 (2006).
[11]M. Li, Y. Sun, H. Xiao, X. Hu, and Y. Yue, Nanotechnology **26**, 105703 (2015).
[12]Y. Xie, Z. Xu, S. Xu, Z. Cheng, N. Hashemi, C. Deng, and X. Wang, Nanoscale **7**, 10101–10110 (2015).
[13]Y. Ma, M. Yu, J. Liu, X. Li, and S. Li, ACS Appl. Mater. Interfaces **9**, 27127–27134 (2017).
[14]X. Cao, Y. Shi, W. Shi, G. Lu, X. Huang, Q. Yan, Q. Zhang, and H. Zhang, Small **7**, 3163–3168 (2011).
[15]J. Liu, L. Zhang, H. Wu, J. Lin, Z. Shen, and X. Lou, Energy Environ. Sci. **7**, 3709–3719 (2014).
[16]B. Y. Zhang, T. Liu, B. Meng, X. Li, G. Liang, X. Hu, and Q. Wang, Nat. Commun. **4**, 1811 (2013).
[17]L. Malard, M. Pimenta, G. Dresselhaus, and M. Dresselhaus, Phys. Rep. **473**, 51–87 (2009).
[18]D. Graf, F. Molitor, K. Ensslin, C. Stampfer, A. Jungen, C. Hierold, and L. Wirtz, Nano Lett. **7**, 238–242 (2007).
[19]J. Guo, X. WeiWang, and T. Wang, J. Appl. Phys. **101**, 063537 (2007).
[20]Y. Xie, S. Xu, Z. Xu, H. Wu, C. Deng, and X. Wang, Carbon **98**, 381–390 (2016).
[21]H. Lin, S. Xu, X. Wang, and N. Mei, Nanotechnology **24**, 415706 (2013).
[22]E. Pop, V. Varshney, and A. K. Roy, MRS Bull. **37**, 1273–1281 (2012).
[23]M. Hu, J. He, Z. Zhao, T. A. Strobel, W. Hu, D. Yu, H. Sun, L. Liu, Z. Li, M. Ma, Y. Kono, J. Shu, H. Mao, Y. Fei, G. Shen, Y. Wang, S. J. Juhl, J. Huang, Z. Liu, B. Xu, and Y. Tian, Sci. Adv. **3**, e1603213 (2017).
[24]T. Tohei, A. Kuwabara, F. Oba, and I. Tanaka, Phys. Rev. B **73**, 064304 (2006).
[25]H. Yang, Y. Li, Y. Yang, D. Chen, and Y. Zhu, Int. J. Heat Mass Transfer **147**, 118974 (2020).
[26]L. Qiu, H. Zou, D. Tang, D. Wen, Y. Feng, and X. Zhang, Appl. Therm. Eng. **130**, 1004–1011 (2018).
[27]H. Wei, H. Bao, and X. Ruan, Nano Energy **71**, 104619 (2020).
[28]X. Xu, L. F. C. Pereira, Y. Wang, J. Wu, K. Zhang, X. Zhao, S. Bae, C. Tinh Bui, R. Xie, J. T. L. Thong, B. H. Hong, K. P. Loh, D. Donadio, B. Li, and B. Özyilmaz, Nat. Commun. **5**, 3689 (2014).
[29]A. A. Balandin, Nat. Mater. **10**, 569 (2011).
[30]Z. Wei, Z. Ni, K. Bi, M. Chen, and Y. Chen, Carbon **49**, 2653–2658 (2011).
[31]S. Ghosh, W. Bao, D. L. Nika, S. Subrina, E. P. Pokatilov, C. N. Lau, and A. A. Balandin, Nat. Mater. **9**, 555 (2010).
[32]W. Yuan, Y. Zhou, Y. Li, C. Li, H. Peng, J. Zhang, Z. Liu, L. Dai, and G. Shi, Sci. Rep. **3**, 2248 (2013).
[33]R. Rozada, J. I. Paredes, S. Villar-Rodil, A. Martínez-Alonso, and J. M. D. Tascón, Nano Res. **6**, 216–233 (2013).
[34]J. Liu, T. Li, Y. Hu, and X. Zhang, Nanoscale **9**, 1496–1501 (2017).
[35]S. Bazrafshan and A. Rajabpour, Int. J. Heat Mass Transfer **123**, 534–543 (2018).
[36]Z. Fan, P. Hirvonen, L. F. C. Pereira, M. M. Ervasti, K. R. Elder, D. Donadio, A. Harju, and T. Ala-Nissila, Nano Lett. **17**, 5919–5924 (2017).
[37]J. Gao, C. Meng, D. Xie, C. Liu, H. Bao, B. Yang, M. Li, and Y. Yue, Appl. Therm. Eng. **150**, 1252–1259 (2019).
[38]X. Fang, X. Yu, H. Zheng, H. Jin, L. Wang, and M. Cao, Phys. Lett. A **379**, 2245–2251 (2015).
[39]D. Nezich, A. Reina, and J. Kong, Nanotechnology **23**, 015701 (2012).
[40]S. Tongay, K. Berke, M. Lemaitre, Z. Nasrollahi, D. B. Tanner, A. F. Hebard, and B. R. Appleton, Nanotechnology **22**, 425701 (2011).
[41]W. Ma, Y. Liu, S. Yan, T. Miao, S. Shi, Z. Xu, X. Zhang, and C. Gao, Nano Res. **11**, 741–750 (2018).